

# Spatiotemporal seismicity pattern of the Taiwan orogen

Yi-Ying Wen<sup>1,2\*</sup>, Chien-Chih Chen<sup>3,4</sup>, Strong Wen<sup>1,2</sup>, and Wei-Tsen Lu<sup>1</sup>

<sup>1</sup>Department of Earth and Environmental Sciences, National Chung Cheng University, Chia-yi County 62102, Taiwan

<sup>2</sup>Environment and Disaster Monitoring Center, National Chung Cheng University, Chia-yi County 62102, Taiwan

<sup>3</sup>Department of Earth Sciences, National Central University, Taoyuan City 32001, Taiwan

<sup>4</sup>Earthquake-Disaster & Risk Evaluation and Management Center, National Central University, Taoyuan City 32001, Taiwan

**Correspondence:** Yi-Ying Wen ([yiyingwen@ccu.edu.tw](mailto:yiyingwen@ccu.edu.tw))

## Abstract

We investigate the temporal and spatial seismicity patterns prior to eight  $M > 6$  events nucleating in different regions of Taiwan through a region-time-length algorithm and an analysis of a self-organizing spinodal model. Our results show that the spatiotemporal seismicity variations during the preparation process of impending earthquakes display distinctive patterns corresponding to tectonic settings. Q-type events occur in southern Taiwan and experience a seismic quiescence stage prior to the mainshock. A seismicity decrease of  $2.5 < M < 4.5$  events occurs around the relatively high b-value southern Central Range, which contributes to the accumulation of tectonic stress for preparing for the occurrence of the Q-type event. On the other hand, A-type events occur in central Taiwan and experience a seismic activation stage prior to the mainshock, which nucleates on the edge of the seismic activation area. We should pay attention when accelerating seismicity of  $3 < M < 5$  events appears within the low b-value area, which could promote the nucleation process of the A-type event.

## 30 **1. Introduction**

31 Seismic activity is related to spatiotemporal variations in the stress field and state,  
32 and seismicity changes prior to a large earthquake have been widely observed through  
33 different techniques, e.g., b-value analysis (Chan et al., 2012; Wyss and Stefansson,  
34 2006), noncritical precursory accelerating seismicity theory (PAST) (Mignan and  
35 Giovambattista, 2008), pattern informatics (PI) algorithm (Rundle et al., 2003; Chen et  
36 al., 2005), the region-time-length (RTL) algorithm (Chen and Wu, 2006; Wen et al.,  
37 2016), and the analysis of self-organizing spinodal (SOS) model (Rundle et al., 2000).  
38 Previous studies have mostly focused on a significant earthquake; therefore, it is not  
39 easy to understand whether the properties of seismic activation and quiescence patterns  
40 respond to regional tectonic stress.

41 The Taiwan orogenic belt, which is an active and ongoing arc–continent collision  
42 zone as a result of the Philippine Sea Plate (PSP) obliquely colliding with the Eurasian  
43 Plate (EP), is particularly complex due to the two adjacent subduction zones, the Ryukyu  
44 trench and Manila trench to the northeast and south of the island, respectively (Suppe,  
45 1984; Yu et al., 1997). The frequent and significant seismic activities as well as a rapid  
46 convergence rate of 85 to 90 mm/yr are well observed by the island-wide GPS and  
47 seismic networks (Fig. 1). The growth of the Taiwan orogenic belt shows propagation  
48 from north to south due to oblique plate convergence and opposing subduction in the  
49 southern and northern parts of Taiwan (Suppe, 1984). The central part of Taiwan, which  
50 is experiencing rapid to full collision, mainly consists of the Coastal Range, Central  
51 Range and Western Foothills (Shyu et al., 2005a; b). A myriad of active and thin-skinned  
52 structures are the products of the accretion of the continental sliver to the continental  
53 margin. In southern Taiwan, the EP subducting eastward beneath the PSP is in a stage  
54 of incipient arc–continent collision (Kao et al., 2000; Shyu et al., 2005a; b). The

55 northwest domain of southern Taiwan, which represent the southern tip of the fold-and-  
56 thrust belt in the coastal plain and foothill region and show very low seismicity, mainly  
57 consist of Miocene shallow marine deposits and a Pliocene–Pleistocene foreland basin  
58 as well as mudstones.

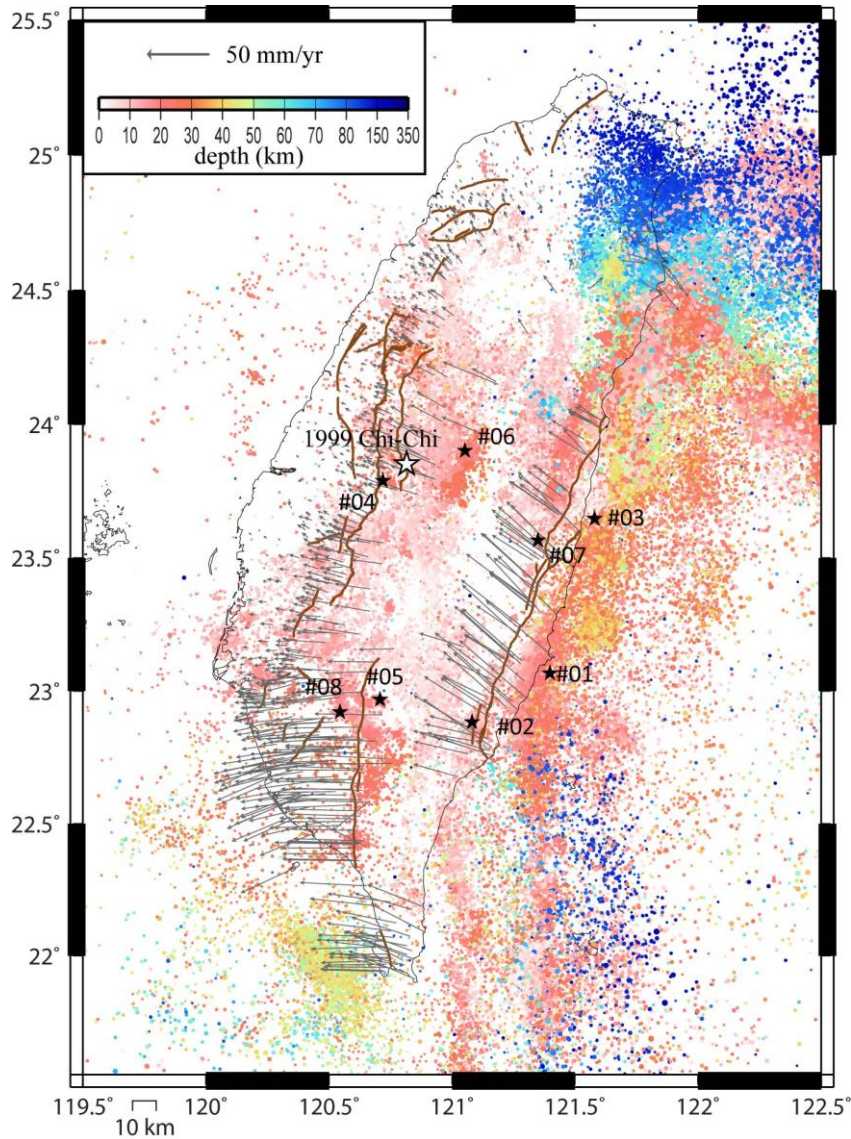


**Figure 1:** Horizontal velocities from 2002 to 2017 (Chen et al., 2018) and seismicity between 1991 and 2018. The white star shows the location of the 1999 Chi-Chi earthquake, and the black stars represent the locations of the investigated events in this study. The active faults (thick lines) identified by the Central Geological Survey of Taiwan are also shown.

59

60 Over the last two decades, several moderate earthquakes have occurred with various

61 seismicity patterns and in GPS velocity field regions. We investigate the temporal and

62 spatial seismicity patterns prior to eight  $M > 6$  events nucleated in different regions of  
 63 Taiwan through the RTL algorithm and analysis of the SOS model. Our attempt is not  
 64 to catch the seismic precursor but to focus on the seismicity changes related to the  
 65 regional tectonics, which might become useful hints for potential seismic hazard  
 66 assessments. The results show that the temporal and spatial seismicity ( $2.5 < M < 5$ )  
 67 variations during the preparation process of impending earthquakes could display  
 68 distinctive patterns corresponding to the tectonic setting.

69

## 70 2. RTL Algorithm and Data

71 The region-time-length (RTL) algorithm (Sobolev and Tyupkin, 1997; 1999) is a  
 72 statistical technique to detect the occurrence of seismic quiescence and activation by  
 73 taking into account the location, occurrence time and magnitude of earthquakes. The  
 74 RTL value is defined as the product of the three dimensionless factors,  $R$ ,  $T$  and  $L$ :

$$75 \quad R(x, y, z, t) = \left[ \sum_{i=1}^n \exp\left(-\frac{r_i}{r_0}\right) \right] - R_{bk}(x, y, z, t) \quad (1)$$

$$76 \quad T(x, y, z, t) = \left[ \sum_{i=1}^n \exp\left(-\frac{t-t_i}{t_0}\right) \right] - T_{bk}(x, y, z, t) \quad (2)$$

$$77 \quad L(x, y, z, t) = \left[ \sum_{i=1}^n \left(\frac{l_i}{r_i}\right) \right] - L_{bk}(x, y, z, t) \quad (3)$$

78 where  $r_i$  is the distance between the investigated point  $(x, y, z)$  and the  $i$ th prior event  
 79 (with the occurrence time  $t_i$  and rupture length  $l_i$ ).  $n$  is the number of prior events that  
 80 occurred in a defined space–time window with  $r_i \leq 2r_0$  ( $r_0$ , characteristic distance) and  
 81  $(t - t_i) \leq 2t_0$  ( $t_0$ , characteristic time-span). Rupture length  $l_i$  is a function of  
 82 earthquake magnitude ( $M_i$ ),  $\log l_i = 0.5M_i - 1.8$  (Kasahara, 1981). The weighted RTL  
 83 value reflects the deviation from the background seismicity level ( $R_{bk}$ ,  $T_{bk}$  and  $L_{bk}$ ) with  
 84 negative values for seismic quiescence and positive values for activation.  $r_0$   
 85 characterizes the decreasing influence of more distant events, and  $t_0$  describes the

86 reducing influence rate of the preceding events as the time of calculation moving on. To  
87 diminish the ambiguity in determining the characteristic parameters, we follow the  
88 systematic procedure of correlation analysis over pairs of RTL results proposed by  
89 Huang and Ding (2012) to obtain the optimal model parameters,  $\tilde{r}_0$  and  $\tilde{t}_0$ , of each  
90 event. Details of this technique of correlation analysis are described in Appendix A. We  
91 calculate various combinations of  $r_0$  (ranging between 25 and 80 km with a step of 2.5  
92 km) and  $t_0$  (ranging between 0.25 and 2.0 yr with a step of 0.05 yr). As the correlation  
93 coefficient criterion  $C_0$  is set, we can calculate the ratio  $W$  (or weight) of the combination  
94 with correlation coefficients equal to or larger than  $C_0$  for each model parameter of  $r_{0i}$   
95 ( $i=1\sim m; m=23$ ) and  $t_{0j}$  ( $j=1\sim n; n=36$ ).

96 After testing many criterion sets, the criterion coefficient  $C_0 = 0.6$  and criterion ratio  
97  $W_0 = 0.5$  are acceptable for each event, which represents at least 50% of the total  
98 combination pairs with correlation coefficient  $C \geq C_0 = 0.6$ . Then, we obtain the average  
99  $\tilde{r}_0 = 49.6$  km and average  $\tilde{t}_0 = 1.16$  yr. These model parameters are similar to those of  
100 previous studies for Taiwan (Chen and Wu, 2006; Wen et al., 2016; Lu, 2017; Wen and  
101 Chen, 2017).

102 For statistical analyses, catalog completeness is an important factor. Since 1991,  
103 the Taiwan Telemetered Seismographic Network (TTSN) (Wang, 1989) has merged  
104 with the Central Weather Bureau (CWB) seismic network and updated to an integrated  
105 earthquake observation system, named the Central Weather Bureau Seismic Network  
106 (CWBSN). Wang et al. (1994) pointed out that most shallow earthquakes occurring in  
107 Taiwan are distributed at depths less than 35 km. According to previous studies (Wu  
108 and Chiao, 2006; Wu et al., 2008; Wen et al., 2016; Hsu et al., 2021), we used the  
109 earthquake catalog maintained by the CWB for the entire Taiwan area with  $M \geq 2.5$  and  
110  $\text{depth} \leq 35$  km between 1991 and 2018 and applied a declustering procedure proposed by

111 Gardner and Knopoff (1974). Considering a sufficient background seismicity and  
 112 minimizing the influence of the 1999 Chi-Chi earthquake, we only selected the  $M>6$   
 113 inland earthquakes between 2003 and 2016 in Taiwan. Since two events occurring in a  
 114 close space–time window would show high similarity in RTL function (Lu, 2017), we  
 115 excluded the event occurring within  $2\tilde{t}_0$  and  $\tilde{r}_0$  with respect to the last  $M>6$  events. For  
 116 example, two  $M>6$  events within a distance of 10 km struck the Nantou area on 27  
 117 March 2013 and 02 June 2013, and we only analyzed the former event. Therefore, we  
 118 have eight qualified  $M>6$  events, as listed in Table 1.

119

120 **Table 1:** Earthquake parameters for the investigated events determined by the CWB.

No.	Date (UT)	Long. (deg.)	Lat. (deg.)	Depth (km)	$M_L$
1	2003/12/10 04:38:14	121.398	23.067	17.7	6.4
2	2006/04/01 10:02:20	121.081	22.884	7.2	6.2
3	2009/10/03 17:36:06	121.579	23.648	29.2	6.1
4	2009/11/05 09:32:58	120.719	23.789	24.1	6.2
5	2010/03/04 00:18:52	120.707	22.969	22.6	6.4
6	2013/03/27 02:03:20	121.053	23.902	19.4	6.1
7	2013/10/31 12:02:10	121.349	23.566	15.0	6.4
8	2016/02/05 19:57:26	120.544	22.922	14.6	6.6

121

## 122 3. Results

### 123 3.1 Temporal seismicity variation

124 The temporal variation in the RTL function represents the different stages of  
 125 seismicity rate change at the target location with respect to the background level. For  
 126 consistency, we adopt a 10-year catalog as the background for each investigated event.  
 127 Figure 2 shows the temporal variation in the RTL functions prior to the investigated

128 events. We can see that before the occurrence of the investigated event, both seismicity  
 129 changes are observed: the seismic quiescence stage for Nos. 1, 2, 5 and 8 (Q-type events  
 130 hereafter) and the seismic activation stage for Nos. 3, 4, 6 and 7 (A-type events hereafter).  
 131 Q-type events occurred at different locations in southern Taiwan, and most, 3 among 4,  
 132 of their temporal RTL functions exhibit the seismic quiescence stages during 2002–  
 133 2004, which was before the occurrence of the 2003 Chengkung earthquake, i.e., event  
 134 No. 1. The seismicity increase (activation stage) took approximately two years following  
 135 the 2003 Chengkung mainshock (event No. 1). We note that the length of the seismic  
 136 quiescence stage prior to the Q-type event might correspond to the magnitude.

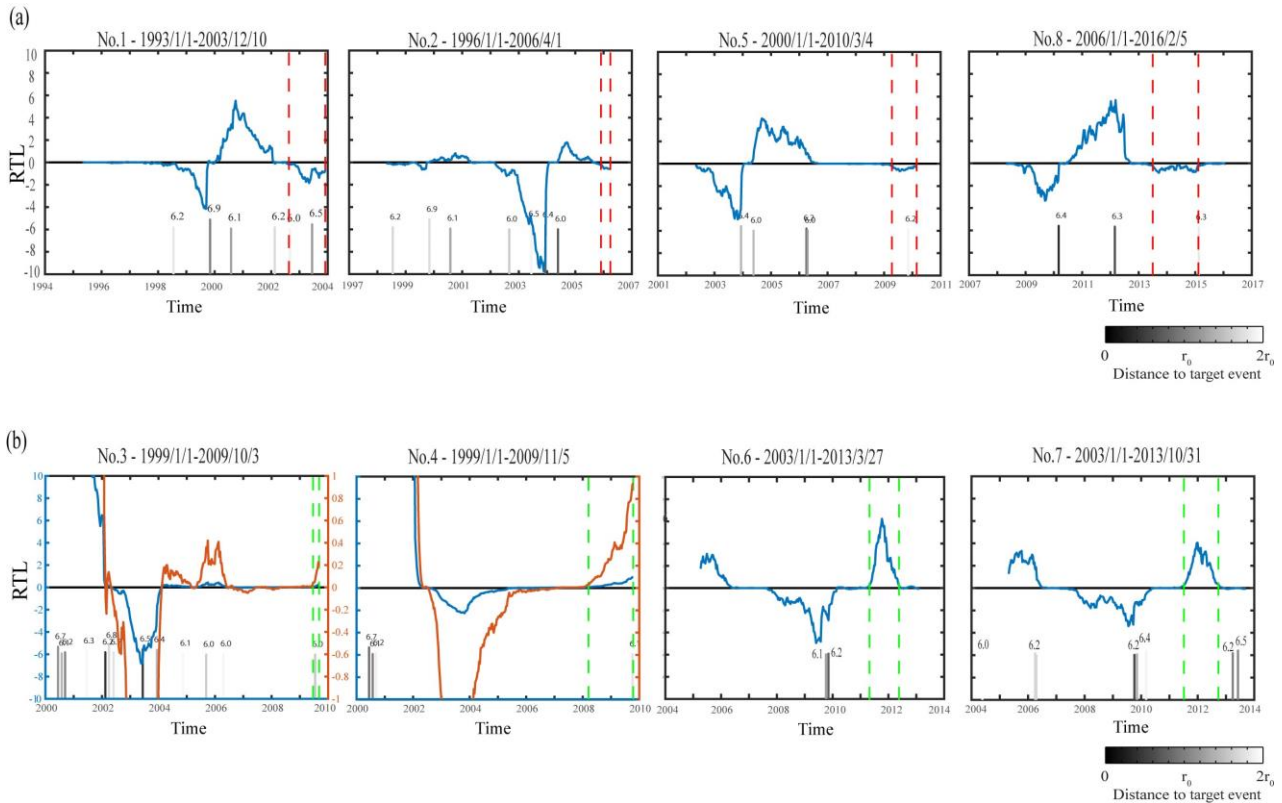


**Figure 2:** Temporal variation of the RTL function (blue line) for (a) Q-type events and (b) A-type events. The orange curves and vertical axes on the right represent the enlarged RTL functions of event Nos. 3 and 4. The vertical dashed red lines mark the seismic quiescence stage, and the vertical dashed green lines mark the seismic activation stage. The bar chart represents the occurrence time of  $M \geq 6.0$  events within a distance of  $2r_0$  from the target event; each number above the bar is the magnitude.

137



138 A-type events all occurred in central Taiwan and were located within  $2\tilde{r}_0$  with  
 139 respect to the 1999 Chi-Chi earthquake. Figure 3 shows the declustered seismicity  
 140 distribution as a function of time and latitude. Significant seismicity followed the 1999  
 141 Chi-Chi earthquake north of  $23^\circ\text{N}$ . Since the background seismicity of event Nos. 3 and  
 142 4 started from 1999/01/01, the RTL functions were obviously affected by the occurrence  
 143 of the 1999 Chi-Chi earthquake. Therefore, we enlarge the vertical axis to accentuate  
 144 the seismicity variation prior to event Nos. 3 and 4. As shown in Fig. 2, the temporal  
 145 RTL functions of A-type events mostly show a seismic activation stage between 2004  
 146 and 2006, which corresponds to the seismicity increase following the 2003 Chengkung  
 147 mainshock (event No. 1). However, for the A-type event, we could not see the  
 148 relationship between the length of the seismic activation stage and the magnitude.

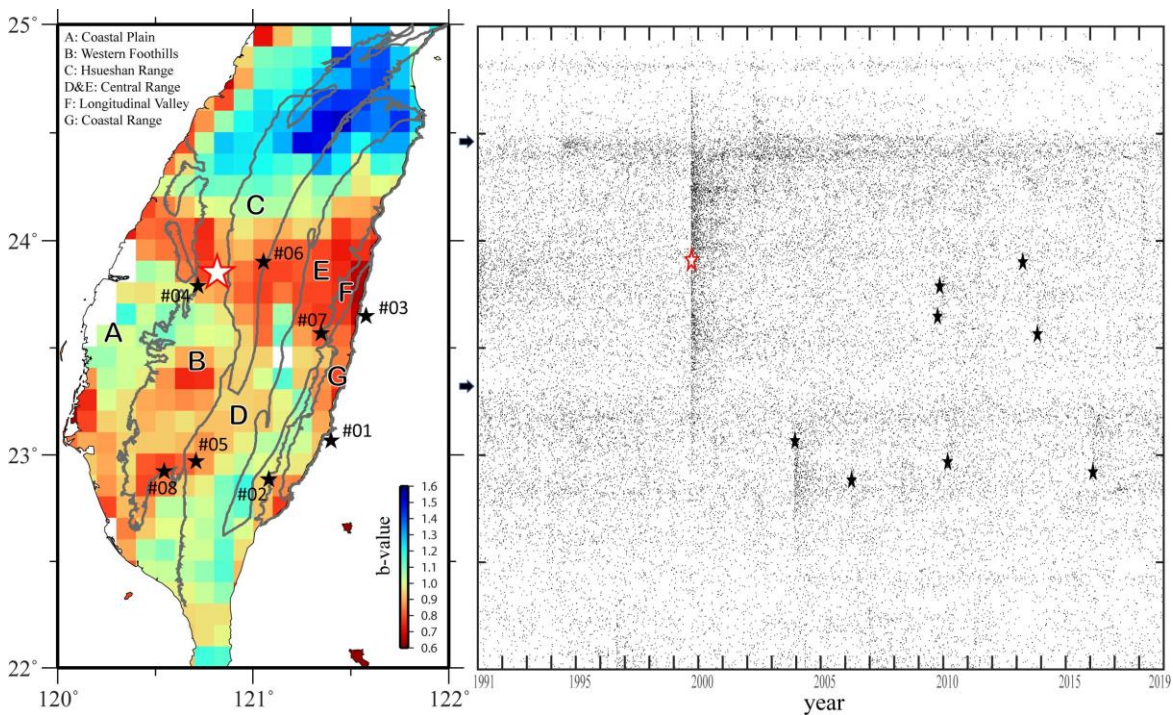


**Figure 3:** Map view of the earthquake b-value and declustered seismicity distribution as a function of time and latitude. The white star indicates the 1999 Chi-Chi earthquake, and the black stars represent the investigated events in this study. The black arrows indicate the seismicity boundaries. The major geological units in Taiwan are marked by gray curves and labeled from A to G.

149

150 **3.2 Spatial Seismic Activation/Quiescence Distribution**



151 Since Q-type and A-type events are located in southern and central Taiwan,  
152 respectively, it would be worth examining the spatial pattern of their abnormal  
153 seismicity stages. Wen and Chen (2017) pointed out that various seismic activation or  
154 quiescence processes of about 2–4 years were found prior to some events occurring in  
155 Taiwan (Chen and Wu, 2006; Wen et al., 2016; Wu et al., 2008). Thus, for consistency,  
156 we only consider the last abnormal stage within four years prior to the investigated  
157 events, as marked by red vertical lines for the quiescence stage of Q-type events and  
158 green vertical lines for the activation stage of A-type events. Then, we calculate the  
159 summation of the selected period to generate the seismic quiescence/activation  
160 distribution. Considering the definition of the weighted RTL function, a sufficient  
161 amount of background seismicity should be regarded as a criterion (Wen and Chen,  
162 2017). Using the declustered catalog from 1991 to 2016, we set up two conditions  
163 similar to those of Wen and Chen (2017) for each grid to strengthen the reliability: (i)  
164 the total number of events within the grid area of  $0.1^\circ \times 0.1^\circ$  must be more than 26 (i.e.,  
165 at least 1 event occurred every year on average); and (ii) the total events within a circle  
166 of  $2r_0$  in radius must be more than 9360 (i.e., at least 30 events occurred every month  
167 on average). For each event, we normalize the spatial distribution based on the summed  
168 result. The spatial seismic activation/quiescence map provides the information of  
169 influence of surrounding seismicity state to the target event during the abnormal stage.  
170 Similar to previous studies (e.g., Huang et al., 2001; Huang and Ding, 2012), Fig. 4  
171 shows that Q-type events mostly occurred on the edge of the seismic quiescence area;  
172 and seismic activation appeared around the A-type events.

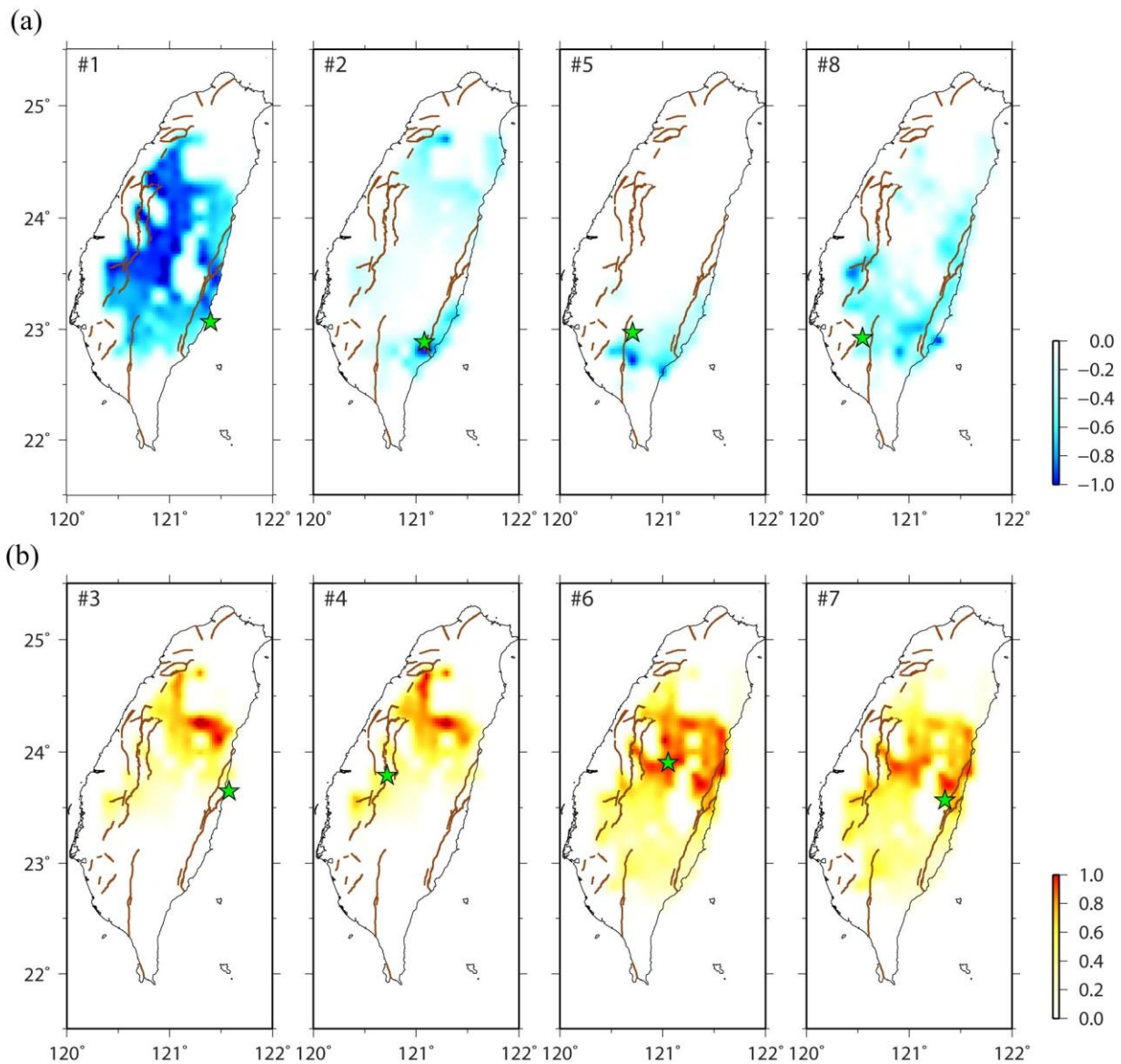


**Figure 4:** (a) The summed and normalized seismic quiescence map for the selected time window of the temporal RTL function of Q-type events, and (b) the summed and normalized seismic activation map for the selected time window of the temporal RTL function of A-type events. Stars represent the locations of the investigated events. The active faults (thick lines) identified by the Central Geological Survey of Taiwan are also shown.

173

174 **4. Discussion**

175 **4.1 Spatiotemporal Characteristics of Seismicity Changes**

176 The RTL analysis accounts for the background seismicity prior to the investigated  
 177 event. Therefore, the RTL analyses account for almost the same background period for  
 178 event Nos. 3 and 4 (1999-2009) and for event Nos. 6 and 7 (2003-2013), respectively.

179 As the temporal RTL functions show the seismic activation stage prior to the  
180 mainshocks during a similar period, we could expect similar seismic activation maps for  
181 event Nos. 3 versus 4 and event Nos. 6 versus 7, as shown in Fig. 4. Furthermore, the  
182 seismic quiescence stage of event No. 5 occurred in a similar period as the seismic  
183 activation stage of event No. 3 (Fig. 2), and the seismic quiescence area of event No. 5  
184 complements the seismic activation area of event No. 3 (Fig. 4). In contrast, although  
185 event Nos. 3 and 7 occurred at close locations, the difference in the 10-year background  
186 period affects the weighting of the deviation. For example, the seismic quiescence stage  
187 during 2007–2009 shown in the temporal RTL function of event No. 7 (Fig. 2) is  
188 evaluated as the background seismicity level (RTL value is equal to zero) in the temporal  
189 RTL function with respect to event No. 3. On the other hand, Wen and Chen (2017)  
190 pointed out that an abnormal seismic stage derived with various background periods  
191 cannot be produced by chance. The temporal RTL functions of five events (Nos. 1–5 in  
192 Fig. 2) accounting for different background periods all exhibit the seismic quiescence  
193 stage before the occurrence of event No. 1. This phenomenon is consistent with the  
194 seismic quiescence map of event No. 1 (Fig. 4) and the Z-value map of Wu et al. (2008)  
195 in which the seismic activity decreased during 2002–2003 for a large area in Taiwan. In  
196 addition, the widespread seismic activation distribution of Nos. 6 and 7 (Fig. 4) also  
197 responded to the seismic activity increase during 2011–2012 (Nos. 6–8 in Fig. 2).

198 Rundle et al. (2000) proposed the self-organizing spinodal (SOS) model for  
199 characteristic earthquakes and suggested that small earthquakes occurred uniformly at  
200 all times, while the occurrence rate of intermediate-sized earthquakes varied during the  
201 earthquake cycle. Chen (2003) investigated the SOS behavior of the 1999 Chi-Chi  
202 earthquake and proposed the seismic activation of moderate-size ( $5 < M < 6$ ) events prior  
203 to the mainshock. Here, we also calculate the cumulative frequency–magnitude

204 distributions for these eight events using the same catalog periods of the RTL analysis.  
 205 For each investigated event, we only compared the distribution diagrams of the long-  
 206 term (background period) and abnormal seismic stages marked by dashed lines in Fig.  
 207 2, within a radius of 25 km with respect to the epicenter. As shown in Fig. 5, cumulative  
 208 frequency-magnitude distributions of long-term seismicity (red dots) generally exhibit  
 209 linear power law distributions. For the Q-type events, the cumulative frequency  
 210 distributions of the seismic quiescence stage (black dots) appear to lack  $2.5 < M < 4.5$   
 211 events (Fig. 5a), and the lack of a level corresponds to the seismic quiescence  
 212 distribution near the epicenter (Fig. 4). This indicates that within the seismic quiescence  
 213 stage before the occurrence of the Q-type event, the quiescence of  $2.5 < M < 4.5$  activity  
 214 contributes to the accumulation of tectonic stress.

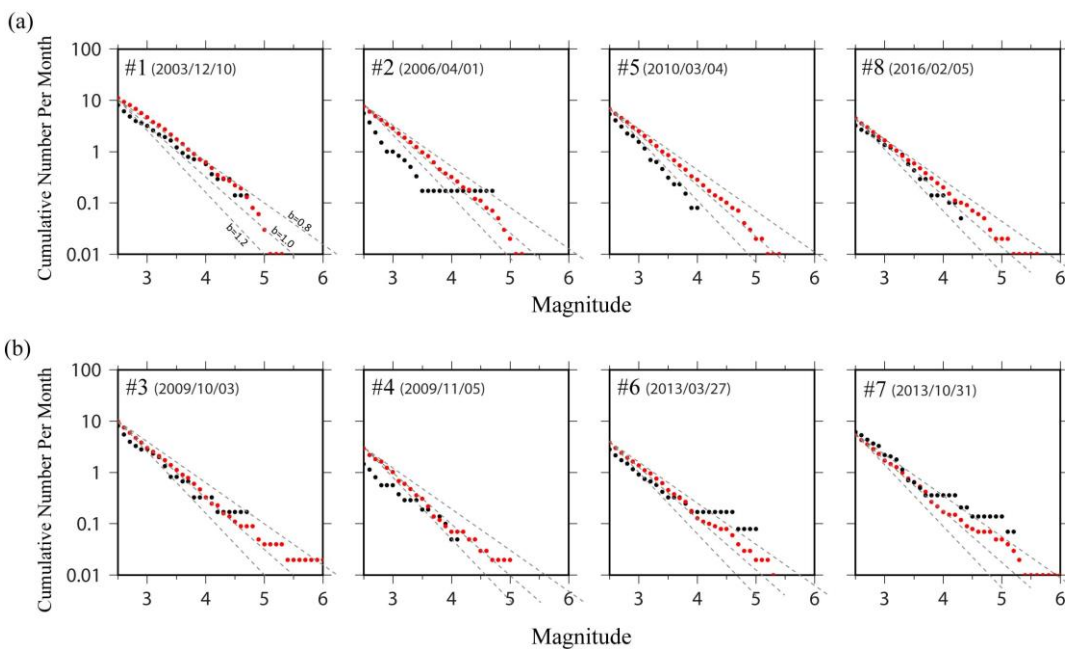


**Figure 5:** The cumulative frequency–magnitude distributions prior to the investigated events. Red and black dots represent the long-term and abnormal seismic stage marked in Fig. 2, respectively.

215

216 On the other hand, the cumulative frequency distributions of the seismic activation stage  
 217 of the A-type events (black dots in Fig. 5b) show that the seismic activation of  $3 < M < 5$   
 218 events within the seismic activation stage before the occurrence of the A-type

219 earthquake can be found, which is similar to the results of the 1999 Chi-Chi earthquake  
220 (Chen, 2003). Event Nos. 6 and 7, which are located very close to the high seismic  
221 activation area (Fig. 4), display the more obvious increase in the number of  $4 < M < 5$   
222 events during the seismic activation stage (Fig. 5b).

223       Event No. 4 occurred only one month later than event No. 3; however, the seismic  
224 activation stage of event No. 4 was much longer than that of event No. 3. Furthermore,  
225 the cumulative frequency distributions of the seismic activation stage of event No. 4  
226 display a lower intercept (Fig. 5b), which represents the overall decreasing seismicity  
227 within this seismic activation stage. Here, we further divide the seismic activation stage  
228 of event No. 4 into three periods for discussion: (i) P1: 2008/02–2009/03 before the  
229 seismic activation stage of event No. 3; (ii) P2: 2009/04–2009/09 matching the seismic  
230 activation stage of event No. 3; and (iii) P3: 2009/10 between the occurrences of event  
231 Nos. 3 and 4. The seismic activation distributions in Fig. 6 are all normalized with  
232 respect to the maximum RTL value of the seismic activation distribution of event No. 4  
233 through Periods P1–P3. We can see that before the seismic activation stage of event No.  
234 3 during 2008/02–2009/03 (P1), the location of event No. 3 indeed shows no seismic  
235 activation, as exhibited in the temporal RTL function (Fig. 2b). On the other hand, for  
236 the location of event No. 4, the seismic activation remains through all three Periods P1–  
237 P3. Combined with the overall decreasing seismicity indicated by the lower intercept in  
238 Fig. 5(b), these results suggest that this seismic activation prior to event No. 4 was  
239 mainly contributed by the relatively accelerating activity of  $3.5 < M < 4$  events.

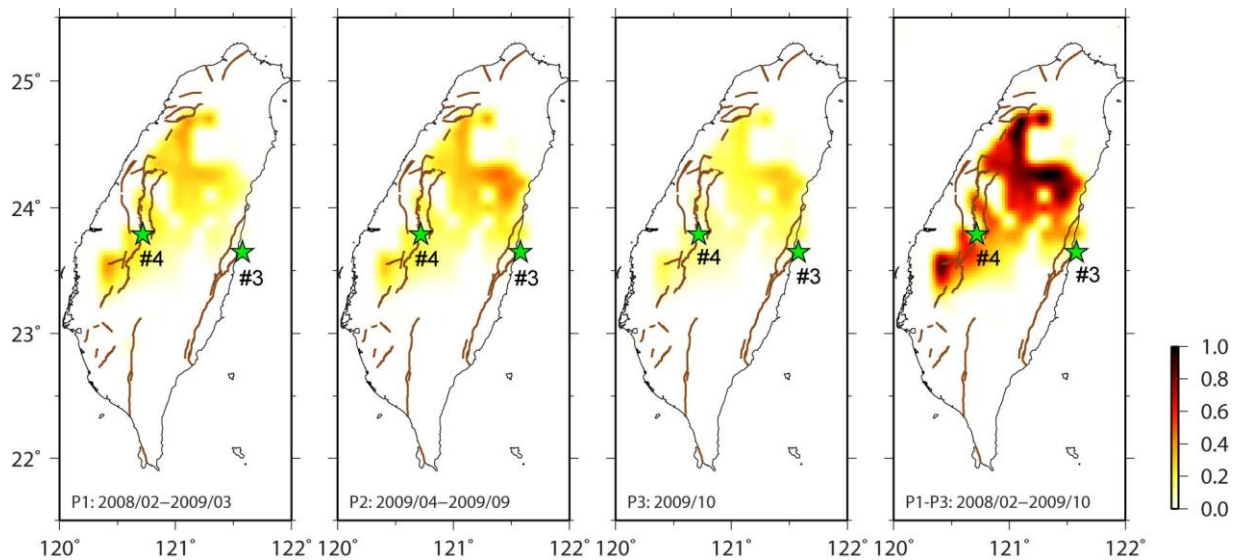


**Figure 6:** The summed seismic activation map for different periods of the seismic activation stage prior to event No. 4; all maps are normalized based on the summed results of P1–P3. Stars represent the locations of event Nos. 3 and 4. The active faults (thick lines) identified by the Central Geological Survey of Taiwan are also shown.

240

#### 241 4.2 Implication for the Tectonic Setting

242 Several major active faults in southwestern Taiwan have been identified, and most  
 243 of them have been dominated by thrust movement. Some strike-slip structures, e.g., the  
 244 Zuochen and Hsinhua faults, acted as the transfer structures between these thrust faults  
 245 (Ching et al., 2011; Deffontaines et al., 1994, 1997; Rau et al., 2012). These transfer  
 246 structures develop at around 23°N, which is the northern limit of the Wadati–Benioff  
 247 zone (Kao et al., 2000) and close to the seismicity boundary indicated in Fig. 3. Geodetic  
 248 data displayed various rates and orientations of horizontal shortening with rapid uplift  
 249 rates in southern Taiwan (Fig. 1), which might be caused by underplating beneath the  
 250 Central Range sustaining crustal thickening and exhumation (Simoes et al., 2007). The  
 251 seismic b-value, which is the relative earthquake size distribution, can be derived from  
 252 the Gutenberg–Richter relation (Gutenberg and Richter, 1944):  $\log N = a - bM$ , where  
 253 constant  $a$  is related to seismicity and  $N$  is the number of earthquakes with magnitudes  
 254 greater than  $M$ . In general, a high b-value indicates a larger proportion of small events,



255 and a low b-value suggests that large earthquakes dominate over small ones. Using the  
256 same declustered catalog from 1991 to 2018, we search for events within a radius of 25  
257 km with respect to the center of each grid ( $0.1^\circ \times 0.1^\circ$ ). Only for the grids with more than  
258 30 events, we calculate the b-value using the weighted least-squares fitting method (Shi  
259 and Bolt, 1982) and the spatial distribution of b-values, as shown in Fig. 3. The  
260 seismicity in the southern Central Range is active but shows significant heterogeneity  
261 in faulting types (Chen et al., 2017; Wu et al., 2018), and relatively high b-values suggest  
262 the predominance of small earthquakes in this region (Fig. 3 and red dots in Fig. 5a; Wu  
263 et al., 2018). Wen et al. (2016) found the decreased seismicity and increased Coulomb  
264 stress change in the southern Central Range prior to the 2010 Jiashian earthquake (i.e.,  
265 event No. 5) and suggested both variations in Coulomb stress and seismicity rate play  
266 important roles in contributing to the nucleation process of impending earthquakes. The  
267 seismicity rate change can be considered a proxy for the stress state change (Dieterich,  
268 1994; Dieterich et al., 2000), and this implies that the quiescence of seismicity  
269 contributes to the accumulation of tectonic stress. Since this relatively high b-value  
270 region in the southern Central Range has been observed to have a seismicity decrease  
271 ( $2.5 < M < 4.5$  events) before the occurrence of Q-type events, it can be an indicator of  
272 stress change.

273 Many devastating earthquakes with surface ruptures have occurred in the central  
274 Taiwan, including the 1935 M 7.1 Hsinchu–Taichung earthquake, the 1951  
275 Longitudinal Valley earthquake sequence and the 1999 Chi-Chi earthquake (Lee et al.,  
276 2007; Chen et al., 2008; Lin et al., 2013). Hsu et al. (2009) derived the consistent  
277 orientations of principal strain-rate and crust stress axes in central Taiwan, which  
278 implies that faulting style corresponds to stress buildup accumulating from interseismic  
279 loading. They also pointed out that, for central Taiwan, small events tend to surround

280 the locked fault zone, where major earthquakes might occur, during the interseismic  
281 period. The 1999 Chi-Chi earthquake ruptured the area near the end of the décollement  
282 with a high contraction rate (Dominguez et al., 2003; Hsu et al., 2003; 2009). In addition,  
283 similar to the 1999 Chi-Chi earthquake, the A-type events occurred in the low b-value  
284 area surrounded by small and active events. Chen and Wu (2006) derived the temporal  
285 RTL function of the 1999 Chi-Chi earthquake, showing a pattern similar to that of A-  
286 type events with the activation stage prior to the mainshock. Furthermore, Wu (2006)  
287 calculated the seismic activation map of the 1999 Chi-Chi event and found that the 1999  
288 Chi-Chi mainshock occurred on the edge of the seismic activation area, which is a low  
289 b-value region. This is similar to the seismic activation maps of A-type events, which  
290 display the hot-spot pattern contracting within the low b-value area (Figs. 3 and 4). The  
291 nucleation of the A-type mainshock can be attributed to the perturbation of background  
292 seismicity ( $3 < M < 5$  events) by the stress state change (Dieterich, 1994; Dieterich et al.,  
293 2000).

294 The cumulative frequency distributions of long-term seismicity in Fig. 5 show a b-  
295 value of 0.8–1.0 around these eight events, which is consistent with the pattern shown  
296 in Fig. 3. However, the cumulative frequency distributions of long-term seismicity  
297 exhibit different trends of magnitudes larger than 4.5 for the two types of events. The  
298 seismicity for  $M > 4.5$  events is lower in the area around the Q-type event but higher in  
299 the area around the A-type event. Event Nos. 1, 2, 3 and 7 occurred in eastern Taiwan  
300 with an average GPS velocity of about 60 mm/yr (Fig. 1), and the cumulative frequency  
301 distributions of long-term seismicity display a high intercept (Fig. 5). This rapid  
302 convergence rate generally remains in the western part of southern Taiwan, which  
303 indicates that only a little shortening is consumed from east to the west in southern  
304 Taiwan. This corresponds to the active seismicity of small earthquakes, as indicated by

305 the high intercept of the cumulative frequency distributions of long-term seismicity for  
306 event Nos. 1, 2, 5 and 8 (Fig. 5). Therefore, for the pre-collisional rapid and  
307 distributed convergence in southern Taiwan (Shyu et al., 2005a), the quiescence of  
308  $2.5 < M < 4.5$  activity contributes to the accumulation of tectonic stress for preparing for  
309 the occurrence of the Q-type event. On the other hand, the shortening rate is obviously  
310 consumed in the mountainous area of central Taiwan. Therefore, the lowest intercept of  
311 the cumulative frequency distributions of long-term seismicity for event No. 4 (Fig. 5)  
312 reflects the slow GPS velocity and low seismicity in the western part of central Taiwan  
313 (Fig. 1). For central Taiwan, small events tend to surround the locked fault zone of the  
314 potential major events during the interseismic period, and the 1999 Chi-Chi earthquake  
315 is the case affected by the accelerating seismicity of moderate-size events and ruptured  
316 the area near the end of the décollement with a high contraction rate (Chen, 2003;  
317 Dominguez et al., 2003; Hsu et al., 2003; 2009). Tectonic stress accumulating from the  
318 interseismic loading with the perturbation of the accelerating activity of  $3 < M < 5$  events  
319 could promote the nucleation process of the A-type event.

320

## 321 **5. Conclusion**

322 Through statistical analyses of recent large earthquakes that occurred in Taiwan, we  
323 summarize various temporal and spatial seismicity patterns prior to the earthquakes that  
324 nucleated in different regions of Taiwan:

- 325 • Q-type events occurred in southern Taiwan, with the northern boundary of  
326  $23.2^{\circ}\text{N}$ , and experienced a seismic quiescence stage prior to the mainshock.  
327 A seismicity decrease of  $2.5 < M < 4.5$  events in the relatively high b-value  
328 southern Central Range could be an indicator of stress change related to the  
329 preparation process of such events.

330           • A-type events occurred in central Taiwan and experienced a seismic  
331           activation stage prior to the mainshock, which nucleated on the edge of the  
332           seismic activation area. We should consider when accelerating seismicity  
333           of  $3 < M < 5$  events appears within the low b-value area.

334           Our results show that the spatiotemporal seismicity variations during the  
335           preparation process of impending earthquakes could display a distinctive pattern  
336           corresponding to the tectonic setting. However, the mechanisms causing these different  
337           phenomena are not clear, and further study is still needed.

338  
339

340 Appendix A

341 In the systematic correlation analysis for searching the optimal model parameters,  
 342 we calculate various combinations of  $r_0$  (ranging between 25 and 80 km with a step of  
 343 2.5 km) and  $t_0$  (ranging between 0.25 and 2.0 yr with a step of 0.05 yr). As the correlation  
 344 coefficient criterion  $C_0$  is set, we can calculate the ratio  $W$  (or weight) of the combination  
 345 with correlation coefficients equal to or larger than  $C_0$  for each model parameter of  $r_{0i}$   
 346 ( $i=1\sim m; m=23$ ) and  $t_{0j}$  ( $j=1\sim n; n=36$ ). Then, the contour map for the ratio  $W$  is generated,  
 347 as shown in Fig. A1.

$$348 \quad W_{ij} = \frac{\sum_{k=1}^m I(C_{ik} \geq C_0) + \sum_{l=1}^n I(C_{jl} \geq C_0)}{m+n} \quad (\text{A1})$$

349 where the logical function  $I(\Phi)$  is defined as

$$350 \quad I(\Phi) = \begin{cases} 1, & \Phi \text{ is true} \\ 0, & \text{otherwise} \end{cases} \quad (\text{A2})$$

351 As the criterion ratio  $W_0$  is set, the optimal model parameters,  $\tilde{r}_0$  and  $\tilde{t}_0$ , can be  
 352 obtained by the following formulas:

$$353 \quad \tilde{r}_0 = \frac{\sum_{j=1}^n \sum_{i=1}^m W_{ij} I(W_{ij} \geq W_0) r_{0i}}{\sum_{j=1}^n \sum_{i=1}^m W_{ij} I(W_{ij} \geq W_0)} \quad (\text{A3})$$

$$354 \quad \tilde{t}_0 = \frac{\sum_{i=1}^m \sum_{j=1}^n W_{ij} I(W_{ij} \geq W_0) t_{0j}}{\sum_{i=1}^m \sum_{j=1}^n W_{ij} I(W_{ij} \geq W_0)} \quad (\text{A4})$$

355 Using event No. 6 as an example, we considered criterion coefficient  $C_0 = 0.6$  and  
 356 criterion ratio  $W_0 = 0.5$ , which indicates that at least 50% of the total combination pairs  
 357 had a correlation coefficient  $C \geq C_0 = 0.6$ . Then, we obtained  $\tilde{r}_0 = 50.0$  km and  $\tilde{t}_0 = 1.14$   
 358 yr (diamond in Fig. A1) by averaging the parameter values that passed the criterion.

359 In addition, Nagao et al. (2011) proposed the RTM algorithm to reduce the dual  
 360 effect of the distance ( $r_i$ ) by introducing the new factor

$$361 \quad M(x, y, z, t) = [\sum_{i=1}^n (M_i)] - M_{bk}(x, y, z, t) \quad (\text{A4})$$

362 where  $M_i$  is the earthquake magnitude of the  $i$ th prior event. Here, we also calculate the  
 363 RTM function of each investigated event with the same characteristic parameter set of  
 364 the RTL model, and both functions display very similar trends with minor differences,  
 365 as shown in Figure R2. The reason for this could be that, for these eight events, no large  
 366 earthquakes occurred in the vicinity of the epicenter. The bar chart in Fig. A2, which

367 represents the occurrence time of  $M \geq 6.0$  events within a distance of  $2r_0$  from the target  
 368 event, also supports this explanation.

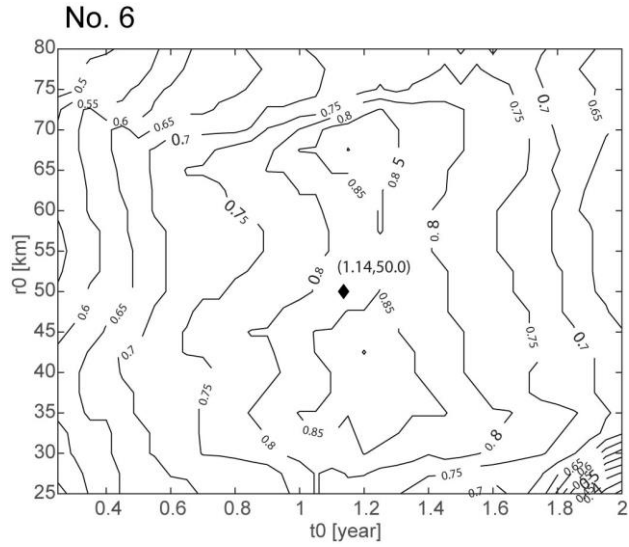


Figure A1: Contour map of ratio  $W$  for various combinations of model parameters of  $r_0$  and  $t_0$ , with  $C_0 = 0.6$  for event No. 6. The diamond shows the optimal model parameters as selecting criterion ratio  $W_0 = 0.5$ .

369  
 370

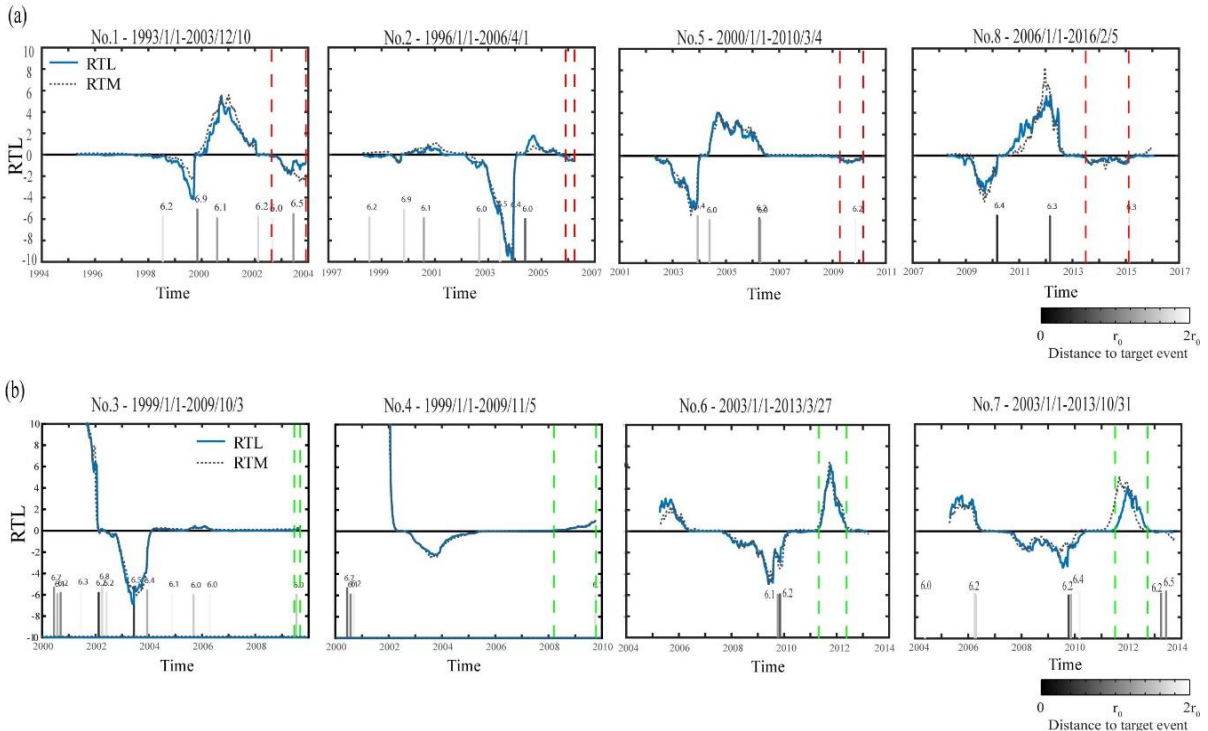


Figure A2: Temporal variation of the RTL (solid line) and RTM (dotted line) functions for (a) A-type events and (b) B-type events. The bar chart represents the occurrence time of  $M \geq 6.0$  events within a distance of  $2r_0$  from the target event; each number above the bar is the magnitude.



371 **Data Availability** : The seismic data is available in the Geophysical Database  
372 Management System (GDMS, <https://gdms.cwb.gov.tw/>). A Chinese manual for data  
373 access from the GDMS is on the website.

374

375 **Author contributions**: Conceptualisation, YYW, CCC; Investigation, YYW, WTL;  
376 Validation, Formal analysis, Writing - original draft preparation, YYW; Writing -  
377 review & editing, YYW, CCC, SW.

378

379 **Competing interests**: The authors declare no conflicts of interest.

380

381 **Acknowledgments**: We thank Central Weather Bureau (CWB) of Taiwan for providing  
382 seismic data. This research was supported by the Ministry of Science and Technology  
383 in Taiwan with grant: MOST 110-2116-M-194-018. The Taiwan Earthquake Center  
384 (TEC) contribution number for this article is \*\*\*\*.

385

386

387 **References:**

- 388 Chan, C.H., Wu, Y.M., Tseng, T.L., Lin, T.L., and Chen, C.C.: Spatial and temporal  
389 evolution of b-values before large earthquakes in Taiwan. *Tectonophysics*, **532**,  
390 215-222, 2012.
- 391 Chen, C.-C., Rundle, J.B., Holliday, J.R., Nanjo, K.Z., Turcotte, D.L., Li, S.C., and  
392 Tiampo, K. F.: The 1999 Chi-Chi, Taiwan, earthquake as a typical example of  
393 seismic activation and quiescence. *Geophys. Res. Lett.*, **32**(22), L22315,  
394 doi:10.1029/2005GL023991, 2005.
- 395 Chen, C.C., and Wu, Y.X.: An improved region–time–length algorithm applied to the  
396 1999 Chi-Chi, Taiwan earthquake. *Geophys. J. Int.*, **166**, 1144-1147, doi  
397 10.1111/j.1365-246X.2006.02975.x, 2006.
- 398 Chen, J.S., Ching, K.E., Rau, R.J., Hu, J.C., Cheng, K.C., Chang, W.L., Chuang, R.Y.,  
399 Chen, C.L., and Chen, H.C.: Surface deformation in Taiwan during 2002-2017  
400 determined from GNSS and precise leveling measurements. Central Geological  
401 Survey Special Publication, 33, 157-178, 2018. (in Chinese with English abstract)
- 402 Chen, K.H., Toda, S., and Rau, R.J.: A leaping, triggered sequence along a segmented  
403 fault: the 1951 Hualien – Taitung earthquake sequence in eastern Taiwan. *J.*  
404 *Geophys. Res.*, **113**, B02304, doi:10.1029/2007JB005048, 2008.
- 405 Chen, S.K., Wu, Y.M., Hsu, Y.J., and Chan, Y.C.: Current crustal deformation  
406 reassessed by cGPS strain-rate estimation and focal mechanism stress inversion.  
407 *Geophys. J. Int.*, **210**, 228–239. <https://doi.org/10.1093/gji/ggx165>, 2017.
- 408 Ching, K.E., Johnson, K.M., Rau, R.J., Chuang, R.Y., Kuo, L.C., and Leu, P.L.: Inferred  
409 fault geometry and slip distribution of the 2010 Jiashian, Taiwan, earthquake is  
410 consistent with a thick-skinned deformation model. *Earth Planet. Sci. Lett.*, EPSL-  
411 S-10-00445, doi:10.1016/j.epsl.2010.10.021, 2011.

412 Deffontaines, B., Lee, J.-C., Angelier, J., Carvalho, J., and Rudant, J.-P.: New  
413 geomorphic data on the active Taiwan orogen: a multisource approach. *J. Geophys.*  
414 *Res.*, **99**, 20243–20266, 1994.

415 Deffontaines, B., Lacombe, O., Angelier, J., Mouthereau, F., Lee, C.T., Deramond, J.,  
416 Lee, J.F., Yu, M.S., and Liu, P.M.: Quaternary transfer faulting in Taiwan Foothills:  
417 evidence from a multisource approach. *Tectonophysics*, **274**, 61–82, 1997.

418 Dieterich, J. H.: A constitutive law for rate of earthquake production and its application  
419 to earthquake clustering. *J. Geophys. Res.*, **99** (18), 2601-2618, 1994.

420 Dieterich, J., Cayol, V., and Okubo, P.: The use of earthquake rate changes as a stress  
421 meter at Kilauea volcano. *Nature*, **408**, 457–460, 2000.

422 Dominguez, S., Avouac, J.P., and Michel, R.: Horizontal coseismic deformation of the  
423 1999 Chi-Chi earthquake measured from SPOT satellite images: implications for  
424 the seismic cycle along the western foothills of central Taiwan. *J. Geophys. Res.*,  
425 **108**, doi:10.1029/2001JB000951, 2003.

426 Gardner, J. K., and Knopoff, L.: Is the sequence of earthquakes in Southern California,  
427 with aftershocks removed, Poissonian?. *Bull. Seis. Soc. Am.*, **64**(5), 1363-1367,  
428 1974.

429 Gutenberg, B., and Richter, C.F.: Frequency of earthquakes in California. *Bull. seism.*  
430 *Soc. Am.*, **34**, 185–188, 1944.

431 Hsu, Y.J., Kao, H., Bürgmann, R., Lee, Y.T., Huang, H.H., Hsu, Y.F., and Zhuang, J.:  
432 Synchronized and asynchronous modulation of seismicity by hydrological loading:  
433 A case study in Taiwan. *Sci. Adv.*, **7** (16), p. eabf7282, doi: 10.1126/sciadv.abf7282,  
434 2021.

435 Hsu, Y.J., Simons, M., Yu, S.B., Kuo, L.C., and Chen, H.Y.: A two-dimensional  
436 dislocation model for interseismic deformation of the Taiwan mountain belt. *Earth*  
437 *Planet. Sci. Lett.*, **211**, 287–294, 2003.

438 Hsu, Y.J., Yu, S.B., Simons, M., Kuo, L.C., and Chen, H.Y.: Interseismic crustal  
439 deformation in the Taiwan plate boundary zone revealed by GPS observations,  
440 seismicity, and earthquake focal mechanisms. *Tectonophysics*, **479**, 4–18.  
441 <https://doi.org/10.1016/j.tecto.2008.11.016>, 2009.

442 Huang, Q., and Ding, X.: Spatiotemporal variations of seismic quiescence prior to the  
443 2011 M 9.0 Tohoku earthquake revealed by an improved Region-Time-Length  
444 algorithm. *Bull. Seismol. Soc. Am.*, **102**(4), 1878-1883, doi: 10.1785/0120110343,  
445 2012.

446 Huang, Q., Sobolev, G.A., and Nagao, T.: Characteristics of the seismic quiescence and  
447 activation patterns before the M=7.2 Kobe earthquake. *Tectonophysics*, **337**, 99-  
448 116, 2001.

449 Kao, H., Huang, G.C., and Liu, C.S.: Transition from oblique subduction to collision in  
450 the northern Luzon arc-Taiwan region: Constraints from bathymetry and seismic  
451 observations. *J. Geophys. Res.*, **105**, 3059-3079, 2000.

452 Kasahara, K.: Earthquake Mechanics, *Cambridge Univ. Press., Cambridge*, 248 pp.,  
453 1981.

454 Lee, S.J., Chen, H.W., and Ma, K.F.: Strong Ground Motion Simulation of the 1999  
455 Chi-Chi, Taiwan, Earthquake from a Realistic 3D Source and Crustal Structure. *J.*  
456 *Geophys. Res.*, **112**, B06307, doi: 10.1029/2006JB004615, 2007.

457 Lin, D.-H., Chen, H., Rau, R.-J., and Hu, J.-C.: The role of a hidden fault in stress  
458 triggering: Stress interactions within the 1935 Mw 7.1 Hsinchu–Taichung

459 earthquake sequence in central Taiwan, *Tectonophysics*. 37-52, doi:  
460 10.1016/j.tecto.2013.04.022, 2013.

461 Lu, W. T.: Seismicity Changes Prior to the M>6 Earthquakes in Taiwan During 1993 to  
462 2016 - an Approach of the RTL Algorithm. M.Sc. thesis, National Chung Cheng  
463 University, Taiwan, p 66, 2017. (in Chinese with English abstract)

464 Mignan, A., and Giovambattista, R. Di: Relationship between accelerating seismicity  
465 and quiescence, two precursors to large earthquakes. *Geophys. Res. Lett.*, **35**,  
466 L15306, doi:10.1029/2008GL035024, 2008.

467 Rau, R.J., Lee, J.C., Ching, K.E., Lee, Y.H., Byrne, T.B., and Chen, R.Y.: Subduction-  
468 continent collision in southwestern Taiwan and the 2010 Jiashian earthquake  
469 sequence. *Tectonophysics*, **578**, 107-116, doi:10.1016/j.tecto.2011.09.013, 2012.

470 Rundle, J.B., Klein, W., Turcotte, D.L., and Malamud, B.D.: Precursory seismic  
471 activation and critical point phenomena. *Pure Appl. Geophys.*, **157**, 2165-2182,  
472 doi:10.1007/PL00001079, 2000.

473 Simoes, M., Avouac, J.P., Beyssac, O., Goffe, B., Farley, K.A., and Chen, Y.G.:  
474 Mountain building in Taiwan: a thermokinematic model. *J. Geophys. Res.*, **112**.  
475 doi:10.1029/2006JB004824, 2007.

476 Shi, Y., and Bolt, B.A.: The standard error of the magnitude-frequency b value. *Bull.*  
477 *seism. Soc. Am.*, **72**, 1677–1687, 1982.

478 Shyu, J. B. H., Sieh, K., and Chen, Y.-G.: Tandem suturing and disarticulation of the  
479 Taiwan orogen revealed by its neotectonic elements. *Earth Planet. Sci. Lett.*, 233,  
480 167–177, 2005a.

481 Shyu, J.B.H., Sieh, K., Chen, Y.-G., and Liu, C.-S.: Neotectonic architecture of Taiwan  
482 and its implications for future large earthquakes. *J. Geophys. Res.*, **110**, p. B08402,  
483 doi: 10.1029/2004JB003251, 2005b.

484 Sobolev, G.A., and Tyupkin, Y.S.: Low-seismicity precursors of large earthquakes in  
485 Kamchatka. *Volc. Seismol.*, **18**, 433-446, 1997.

486 Sobolev, G.A., and Tyupkin, Y.S.: Precursory phases, seismicity precursors, and  
487 earthquake prediction in Kamchatka. *Volc. Seismol.*, **20**, 615-627, 1999.

488 Suppe, J.: Kinematics of arc-continent collision, flipping of subduction, and backarc  
489 spreading near Taiwan. *Mem. Geol. Soc. China*, 21–33, 1984.

490 Wang, J.H.: The Taiwan Telemetered Seismographic Network. *Phys. Earth Planet.*  
491 *Inter.*, **58**, 9–18, 1989

492 Wang, J.H., Chen, K.C., and Lee, T.Q.: Depth distribution of shallow earthquakes in  
493 Taiwan. *J. Geol. Soc. China*, **37**, 125–142, 1994.

494 Wen, Y.-Y., Chen, C.-C., Wu, Y.-H., Chan, C.-H., Wang, Y.-J., and Yeh, Y.-L.:  
495 Spatiotemporal investigation of seismicity and Coulomb stress variations prior to  
496 the 2010 ML 6.4 Jiashian, Taiwan earthquake. *Geophys. Res. Lett.*, **43**,  
497 doi:10.1002/2016GL070633, 2016.

498 Wen, Y.-Y., and Chen, C.-C.: Seismicity variations prior to the 2016 ML 6.6 Meinong,  
499 Taiwan earthquake. *Terr. Atmos. Ocean. Sci.*, **28**, 737-742, doi:  
500 10.3319/TAO.2016.12.05.01, 2017.

501 Wu, Y. H.: An improved region–time–length algorithm applied to the 1999 Chi-Chi,  
502 Taiwan earthquake. M.Sc. thesis, National Central University, Taiwan, p 115, 2006.  
503 (in Chinese with English abstract)

504 Wu, Y.M., and Chiao, L.Y.: Seismic Quiescence before the 1999 Chi-Chi, Taiwan, Mw  
505 7.6 Earthquake. *Bull. Seismol. Soc. Am.*, 96, 321-327, doi: 10.1785/0120050069,  
506 2006.



507 Wu, Y.M., Chen, C.-C., Zhao, L., and Chang, C.-H.: Seismicity characteristics before  
508 the 2003 Chengkung, Taiwan, earthquake. *Tectonophysics*, **457**, 177-182, doi:  
509 10.1016/j.tecto.2008.06.007.

510 Wu, Y.M., Chen, S. K., Huang, T.C., Huang, H.-H., Chao, W.A., and Koulakov, I.:  
511 Relationship between earthquake b-values and crustal stresses in a young orogenic  
512 belt. *Geophys. Res. Lett.*, **45**, 1832-1837, doi:10.1002/2017GL076694, 2018.

513 Wu, Y.M., Hsu, Y.J., Chang, C.H., Teng, L.S., and Nakamura, M.: Temporal and spatial  
514 variation of stress field in Taiwan from 1991 to 2007: Insights from comprehensive  
515 first motion focal mechanism catalog. *Earth Planet. Sci. Lett.*, **298**, 306–316.  
516 <https://doi.org/10.1016/j.epsl.2010.07.047>, 2010.

517 Wyss, M., and Stefansson, R.: Nucleation points of recent mainshocks in Southern  
518 Iceland, mapped by b-values. *Bull. Seismol. Soc. Am.*, **96**, 599–608, 2006.

519 Yu, S.B., Chen, H.Y., and Kuo, L.C.: Velocity field of GPS stations in the Taiwan area.  
520 *Tectonophysics*, **274**(1-3), 41–59. [https://doi.org/10.1016/S0040-1951\(96\)00297-1](https://doi.org/10.1016/S0040-1951(96)00297-1),  
521 1997.

522